

CHAPTER IV

RESULTS AND DISCUSSION

The results and discussion part are divided into two parts: the binary systems and the ternary systems. The binary system consists of the aqueous polymer solutions and the aqueous surfactant solutions. The ternary system consists of the aqueous polymer-surfactant solutions.

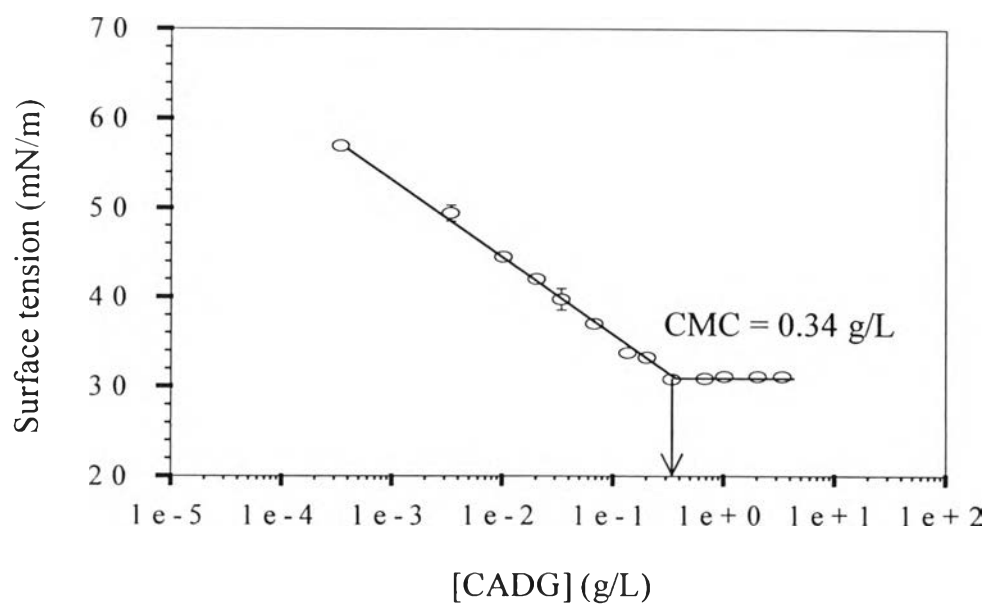
4.1 Binary Systems

4.1.1 The CADG/Water System

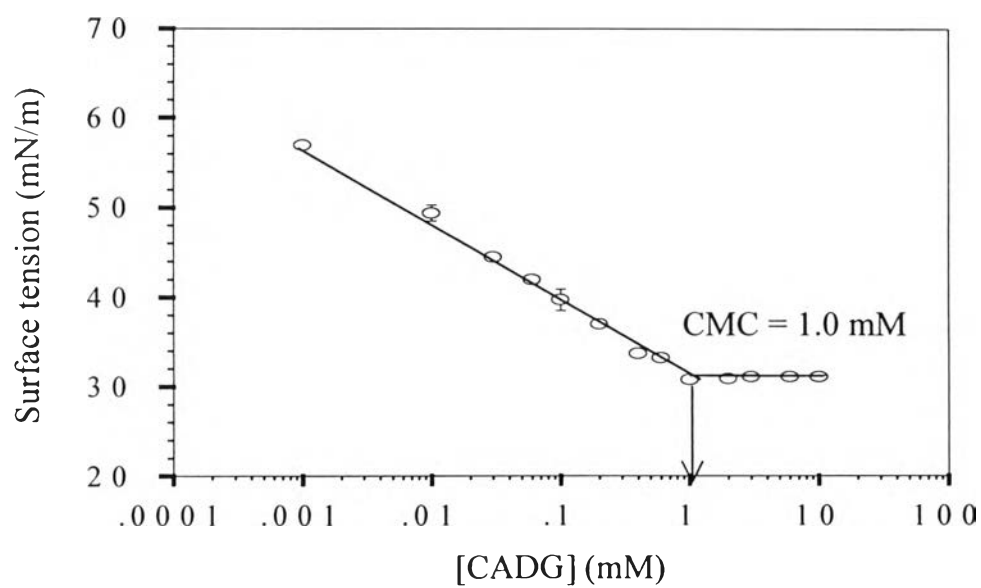
4.1.1.1 The Critical Micelle Concentration Determination

The critical micelle concentration (CMC) of CADG was determined using the surface tension method. The onset of micellization can be determined from a surface tension versus log concentration plot which shows a sharp break at the CMC followed by an almost constant surface tension with increase in surfactant concentration (Goddard and Ananthapadmannabhan, 1993).

Figure 4.1 shows the surface tension of the aqueous CADG solution decreases steadily as the bulk concentration of CADG is increased until the concentration reaches a value known as the CMC, above which the tension remains virtually unchanged. The surface tension at the CMC is therefore very close to the minimum tension that the system can achieve. The CMC of aqueous CADG solution is equal to 0.34 g/L.



(a)



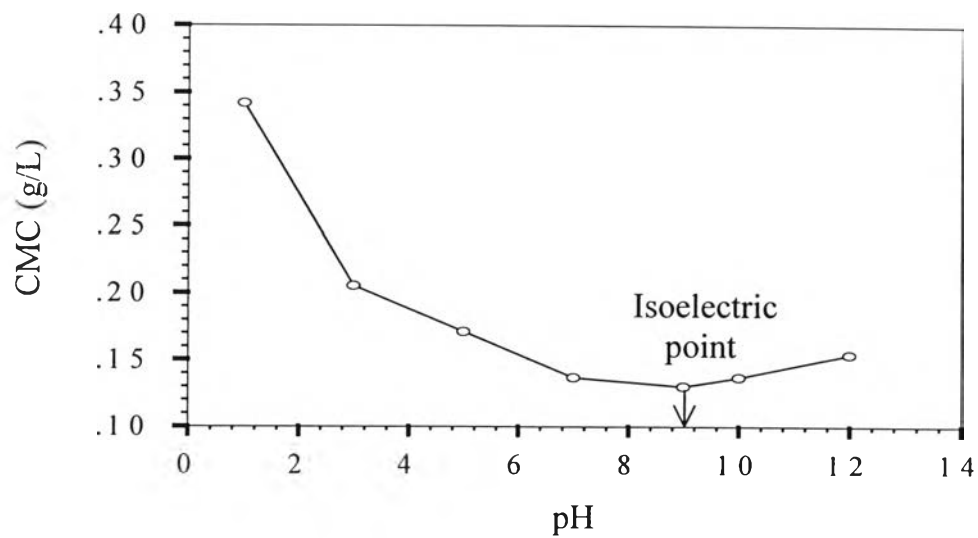
(b)

Figure 4.1 Surface tension versus CADG concentration at 30°C for CADG/water system: (a) CADG concentration in g/L; (b) CADG concentration in mM.

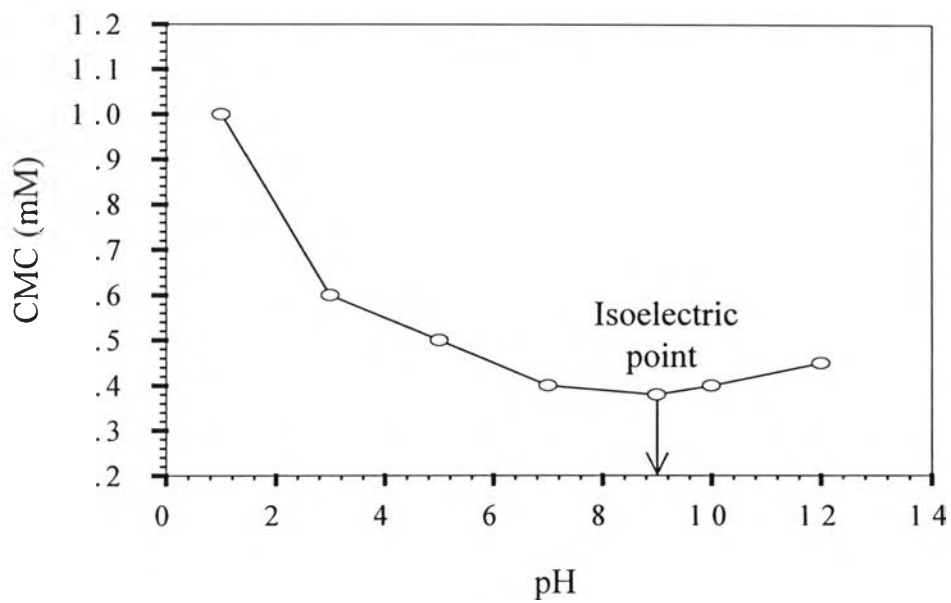
A surfactant molecule has lower energy than a water molecule at the surface. The surfactant therefore concentrates at the surface, since less work is now needed to bring molecules to the surface, the presence of the surfactant decreases the work needed to create unit area of surface (the surface free energy per unit area, or surface tension). However, the distortion of the solvent structure can also be decreased (and the free energy of the solution reduced) by the aggregation of the surfactant molecules into micelles with their hydrophobic groups directed toward the interior of the micelle and their hydrophilic groups directed toward the solvent. Micellization is therefore an alternative mechanism to the adsorption at the interfaces for removing hydrophobic groups from contact with the water, thereby reducing the free energy of the system (Rosen, 1989).

The CMC of an amphoteric surfactant depends on the pH because of the variation in the amount of ionic charges and closeness of packing. The change in the amount of charges gives rise to a change in solubility. At high pH, the amphoteric surfactant will be anionic, with the cationic group having relatively small or no effect. As the pH decreases, the anionic group weakens as the cationic group strengthens until, at the isoelectric area, the solubility is at minimum. Below the isoelectric area the cationic group begins to predominate, and the CMC will rise again (Eric, 1996).

Figure 4.2 shows the CMC of aqueous CADG solutions as a function of pH. From this figure, the CMC shows a minimum at around pH 9.0 which we estimate as the isoelectric point. Below the pH value of 9.0, CMC decreases. Beyond that, CMC slightly increases as a function of pH.



(a)



(b)

Figure 4.2 Critical micelle concentration (CMC) versus pH at 30°C for aqueous CADG solution: (a) critical micelle concentration in g/L; (b) critical micelle concentration in mM.

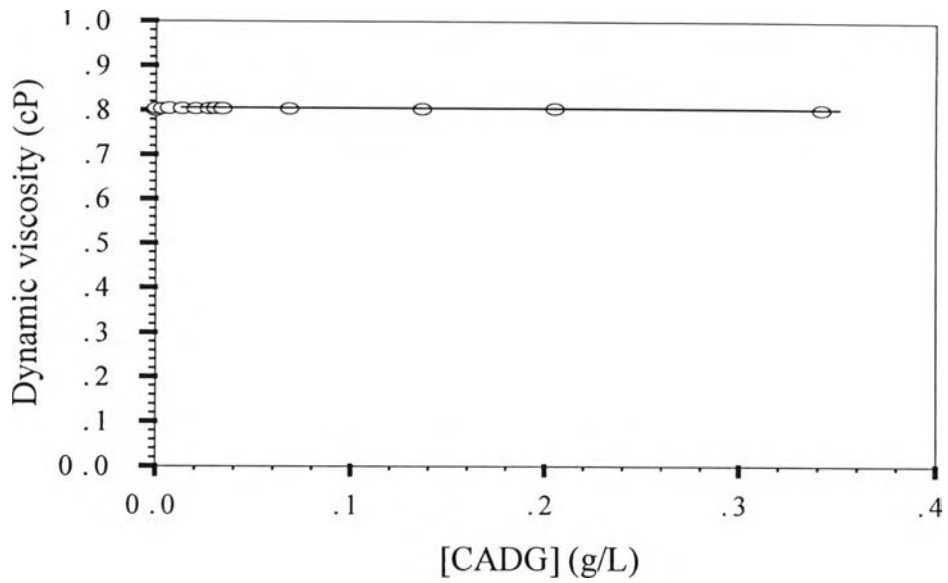
The isoelectric point is the condition in which the net charge is at a minimum, because there are equal numbers of positive and negative charges on the micelles. The cationic group gives rise to a decrease in the repulsion between negative charges, while the anionic group can act to decrease the repulsion between positive charges, promoting closer packing. Then the hydrophilic repulsion is small compared with the hydrophobic attraction of the molecule; and the molecules aggregate easily at low concentration. This means that the CMC is low. Below this pH the CADG behaves progressively more as a cationic surfactant. Therefore, the packing of CADG molecules is made more difficult because of the increase of electrostatic repulsion the CADG molecules. Thus the CMC is high.

4.1.2.2 Viscosity Determination

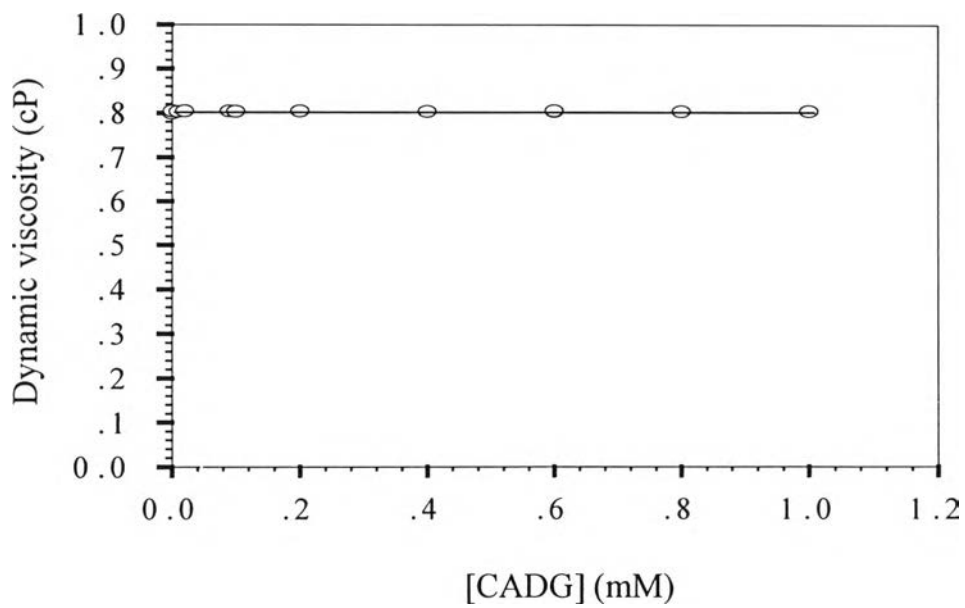
The viscosity determination of aqueous CADG solutions was performed using a Ubbelodhe capillary viscometer of size 50. Figure 4.3 shows the dynamic viscosity of aqueous CADG solution as a function of CADG concentration without pH adjustment. The pH of CADG solution is about 4.5 to 5.5. The dynamic viscosity remains unchanged with the increase in the CADG concentration up to the CMC value. The dynamic viscosity, η_{dynamic} , is defined as the force per unit area necessary to maintain a unit velocity gradient at right angles to the direction of flow between two parallel planes a unit distance apart. The dynamic viscosity can be obtained from equation (4.1):

$$\eta_{\text{dynamic}} = \eta_{\text{kinematic}} \times d_{\text{solvent}} \quad (4.1)$$

where $\eta_{\text{kinematic}}$ is the kinematic viscosity which is equal to $t \times K$, t is the flow time, K is a Ubbelodhe capillary viscometer's constant and d_{solvent} is the density of a solvent (Dean, 1987).



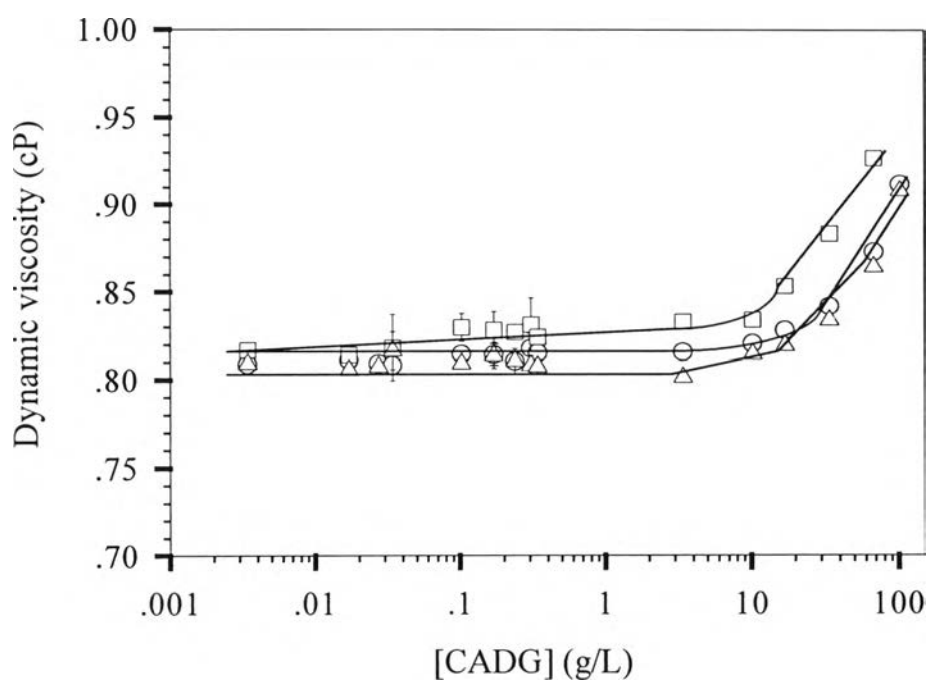
(a)



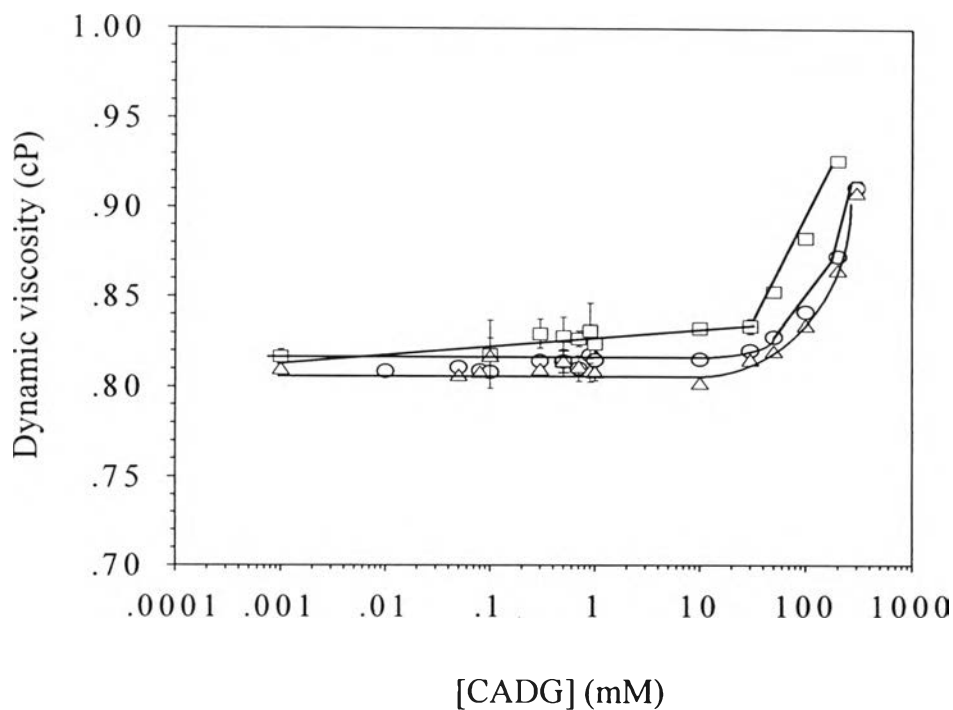
(b)

Figure 4.3 Dynamic viscosity versus CADG concentration at 30°C for CADG/water system: (a) CADG concentration in g/L; (b) CADG concentration in mM.

Figure 4.4 show the dynamic viscosity versus concentration of CADG/water solution at pH equal to 3.0, 7.0 and 12.0. The viscosity remains unchanged with increase in CADG concentration up to about 10 g/L. Beyond that concentration, an addition of CADG concentration gives a dramatic increase in the dynamic viscosity because the surfactant phase volume increases with CADG concentration or the formation of supramicellar structures occurred.



(a)



(b)

Figure 4.4 Dynamic viscosity versus CADG concentration at 30⁰C for CADG/water system: (○) pH 3.0, (□) pH 7.0, (△) pH 12.0, (a) CADG concentration in g/L; (b) CADG concentration in mM.

4.1.2 The HPC/Water System

4.1.2.1 *Viscosity Determination*

The viscosity of the aqueous HPC solutions was determined using the Ubbelohde capillary viscometer of size 50. Figure 4.5 shows the reduced viscosity, η_{sp}/C_{HPC} , and the inherent viscosity, $\ln(\eta_r)/C_{HPC}$, of aqueous HPC solutions versus HPC concentration, C_{HPC} , at 30⁰C. The data suggest a linear dependence of the reduced viscosity and inherent viscosity on HPC concentration. Straight lines can be drawn

through η_{sp}/C_{HPC} versus C_{HPC} and $\ln(\eta_r)$ versus C_{HPC} according to the Huggins equation and the Kraemer equation, respectively. The intrinsic viscosity $[\eta]$ of HPC was determined by intercept of these lines and found to be 0.127 L/g. The inverse intrinsic viscosity, $[\eta]^{-1}$, measures the degree of overlap concentration, c^* , which is the concentration at which polymer chains begin to overlap each other. Then c^* for this aqueous HPC solution is 7.8 g/L. Above this concentration, the polymer solution enters into the semidilute regime.

$$c^* = 1/[\eta] \quad (4.2)$$

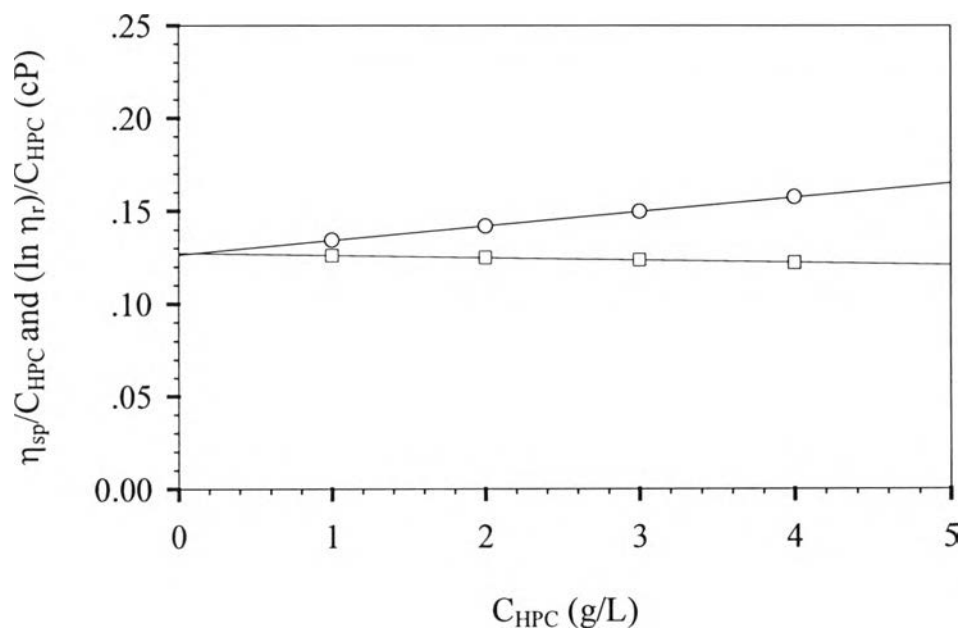


Figure 4.5 Plot of reduced viscosity (η_{sp}/C_{HPC}) and inherent viscosity $(\ln \eta_r)/C_{HPC}$ for aqueous HPC solution as a function of HPC concentration at 30°C: (o) reduced viscosity, (□) inherent viscosity.

4.1.2.2 Hydrodynamic Radius Determination

The hydrodynamic radius was determined using dynamic light scattering. Figure 4.6 shows the apparent diffusion coefficient at the fixed HPC concentration of 2 g/L depends on the scattering wave vector square, q^2 , at scattering angles from 70° to 140° . The scattering wave vector, q , is defined as

$$q = (4\pi n/\lambda) \sin(\theta/2) \quad (4.3)$$

where q is the scattering vector, n is the solvent refractive index, λ is the wavelength and θ is the scattering angle.

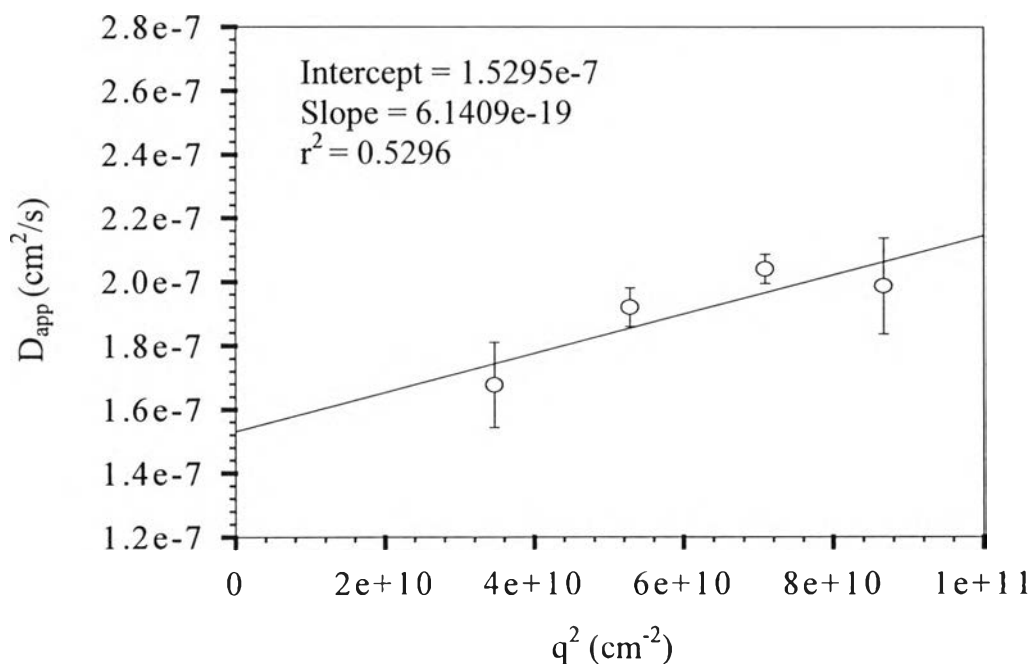


Figure 4.6 Apparent diffusion coefficient at the fixed HPC concentration of 2 g/L for HPC/water system as a function of the scattering wave vector at 30°C .

When the apparent diffusion coefficient in equation (4.4) is extrapolated to zero angle, the center of mass diffusion coefficient, D_c , can be obtained from the intercept (Sun, 1994). Similar plots for other HPC concentrations are shown in Appendix C.

$$D_{app}(q) = D_c(1 + Cq^2R_g^2 - \dots) \text{ for } qR_g < 2 \quad (4.4)$$

Figure 4.7 shows the plot of the center of mass diffusion coefficient of the aqueous HPC solutions versus HPC concentration at 30°C. The diffusion coefficient, D_0 , can be obtained from the intercept as

$$D_c = D_0(1 + k_D c_p) \quad (4.5)$$

where k_D is the diffusion virial coefficient, which is equal to $2A_2M - k_p - V_2$, A_2 is the second virial coefficient, M is molecular weight, k_p is the concentration dependence of the friction coefficient and V_2 is the partial specific volume.

The hydrodynamic radius, R_h , can be determined using the Stoke-Einstein equation, equation (4.6):

$$R_h = k_B T / 6\pi\eta_0 D_0 \quad (4.6)$$

where k_B is the Boltzman constant, η_0 is the solvent viscosity and T is temperature in Kelvin. The hydrodynamic radius of this HPC solution is 21.3 nm that is consistent with Hornmiron *et al* (1999) which is 18.9 nm.

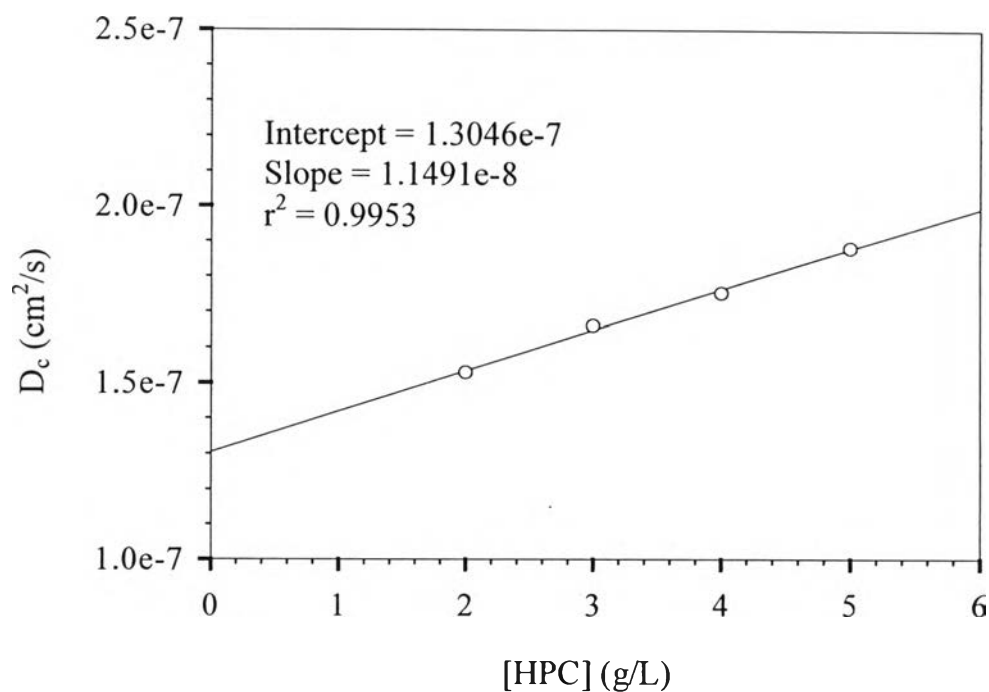


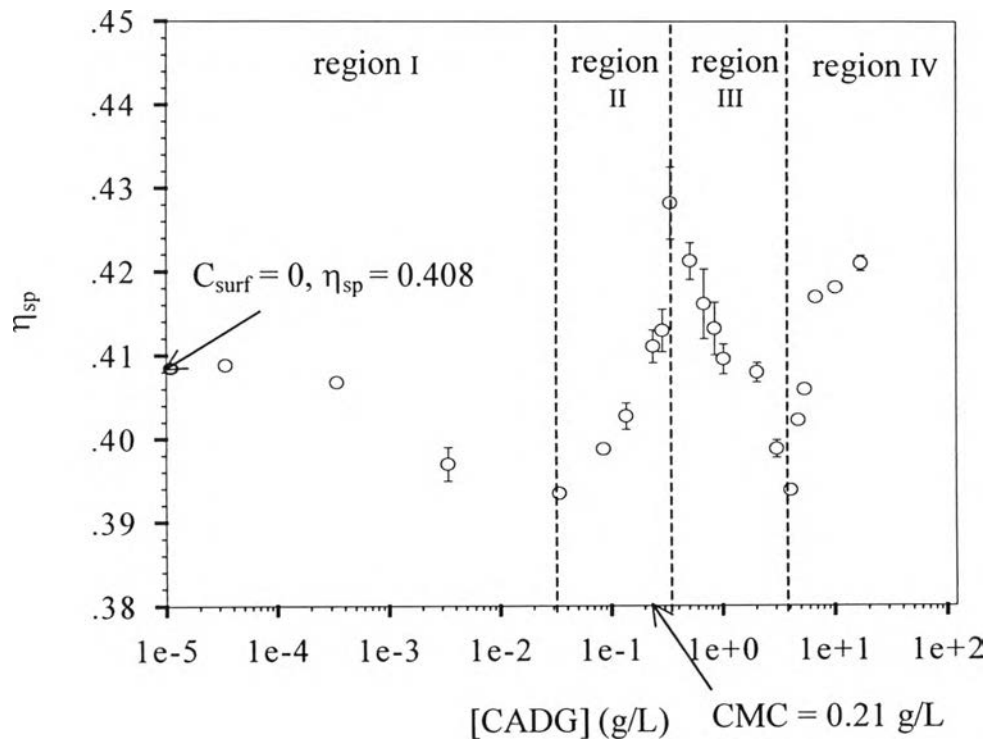
Figure 4.7 Center of mass diffusion coefficient (D_c) as a function of the HPC concentration at 30°C for the aqueous HPC solution.

4.2 Ternary System

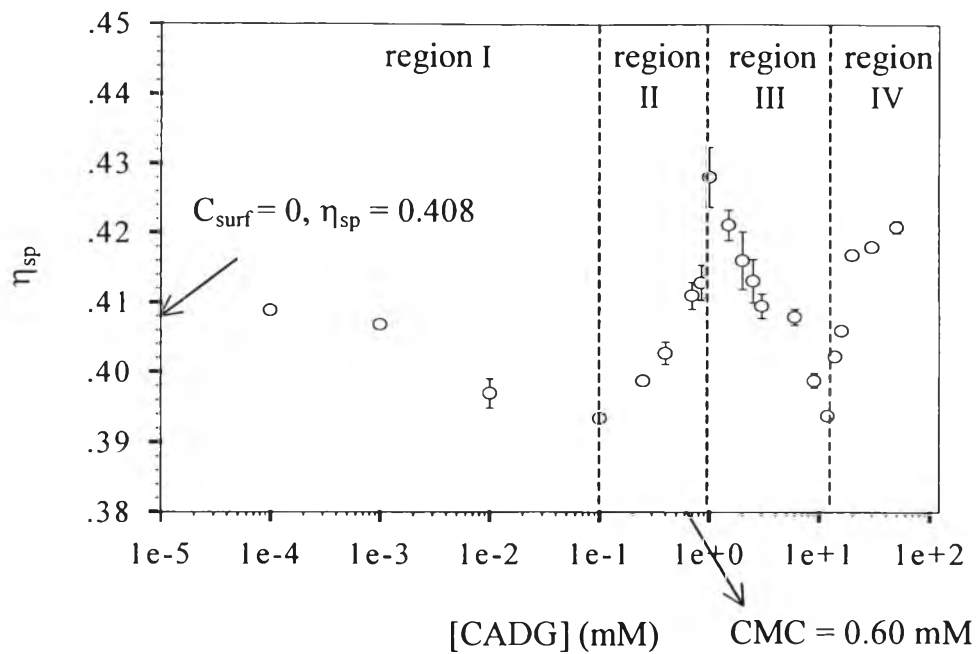
4.2.1 The Viscosity Determination

The viscosity of HPC/CADG/water system was determined using a Ubbelohde capillary viscometer of size 50. Figure 4.8 shows the results from the viscosity measurement at 30°C at pH 3.0 for the HPC/CADG/water system as a plot of the specific viscosity against the CADG concentration. The HPC concentration was fixed at 2.6 g/L while the CADG concentration was varied. This figure can be divided into four regions. In the first region, CADG concentration is between $3.42e-5$ g/L and 0.034 g/L the specific viscosity slightly decreases from 0.408 to 0.392. Then the specific viscosity rapidly increases from 0.392 to 0.429 in region II when the CADG concentration increases from 0.034 g/L to 0.34 g/L. In

region III, where the CADG concentration is between 0.34 g/L and 4.0 g/L, the specific viscosity decreases from 0.429 to 0.394. In the last region, the specific viscosity quickly increases as a function of CADG concentration. The CADG concentration of about 0.34 g/L corresponds to the maximum specific viscosity of about 0.430 which we select as the maximum binding point. A schematic picture of the micellar structures which accompany the change of viscosity is shown in Figure 4.9.



(a)



(b)

Figure 4.8 The specific viscosity of fixed 2.6 g/L of HPC concentration as a function of CADG concentration at 30°C of HPC/CADG/water system at pH 3.0: (a) CADG concentration in g/L; (b) CADG concentration in mM.

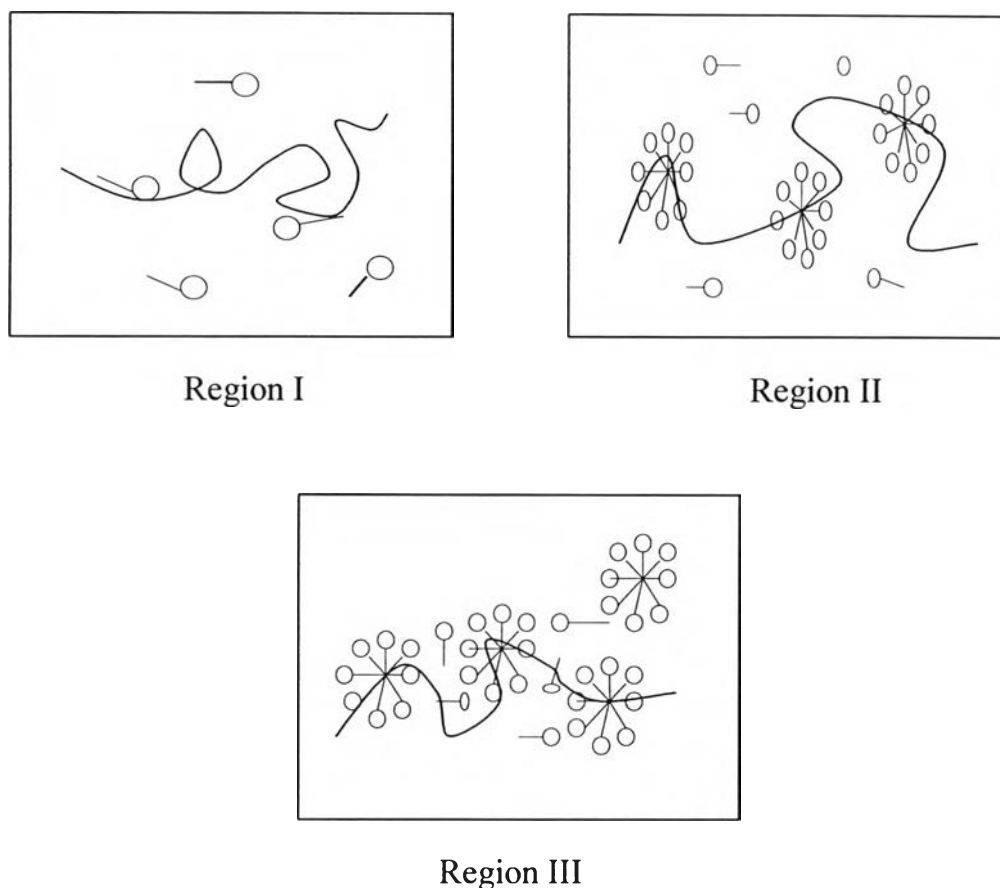


Figure 4.9 Schematic representation of the mechanism for the interaction between HPC and CADG.

Region I : In solutions of HPC containing a low concentration of CADG, the bound CADG molecules make the HPC more hydrophobic and change solvent quality.

Region II: CADG molecules start to bind as a cluster of micelles to HPC chain. The size of HPC chain increases because the electrostatic repulsion of charged micelles.

Region III: After the HPC chain is saturated in region II, the addition of CADG causes the size of HPC-bound CADG clusters to decrease due to the screening effect of counterions.

Figure 4.10 shows the specific viscosity HPC/CADG/water system at pH 12.0 as a function of CADG concentration, the HPC concentration is fixed at 2.6 g/L. This figure can again be classified into four regions. Region I, where the CADG concentration is between 1.71×10^{-8} g/L and 3.42×10^{-4} g/L the specific viscosity rapidly decreases from 0.400 to 0.368. In region II, the specific viscosity rapidly increases from 0.368 to 0.402 when the CADG concentration is between 3.42×10^{-4} g/L and 0.24 g/L. In region III, when the CADG concentration increases from 0.24 g/L to 4.00 g/L, the specific viscosity rapidly decreases from 0.402 to 0.370. Subsequently, the specific viscosity rapidly increases as a function of CADG concentration. At the CADG concentration of about 0.24 g/L the maximum specific viscosity of about 0.402 is observed, corresponding to the maximum binding point.

A difference between Figure 4.8 and Figure 4.10 is that the specific viscosity rapidly decreases in region I for HPC/CADG/water system at pH 12.0, whereas the specific viscosity for HPC/CADG/water system at pH 3.0 decreases only slightly. The specific viscosity for HPC/CADG/water system at pH 12.0 starts to decrease at around 1.71×10^{-8} g/L of CADG concentration while the specific viscosity for HPC/CADG/water system at pH 3.0 start to decrease at around 3.42×10^{-5} g/L of CADG concentration. The maximum viscosity for HPC/CADG/water system at pH 3.0 is about 0.430, which is higher than the maximum viscosity for HPC/CADG/water system pH 12.0, i.e. 0.402.

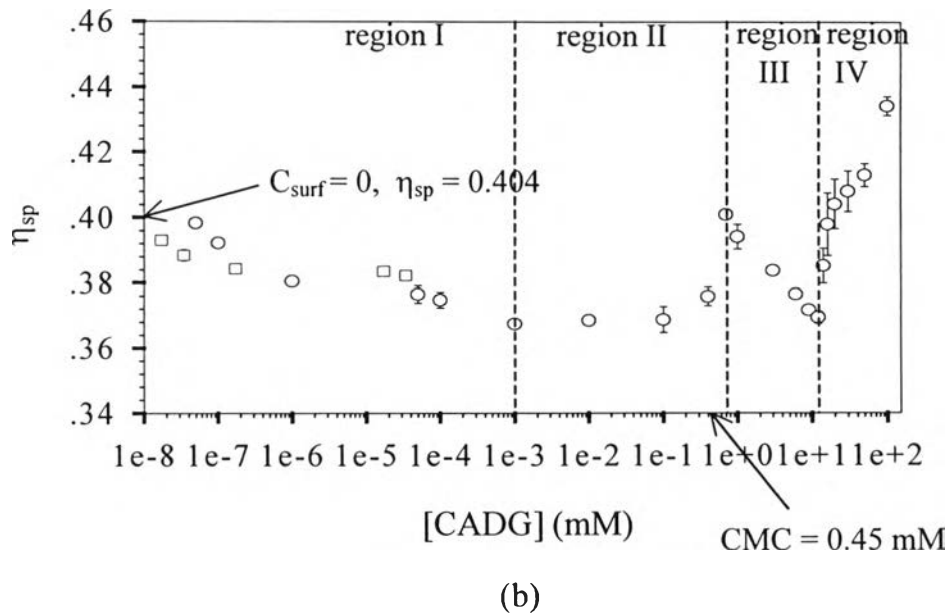
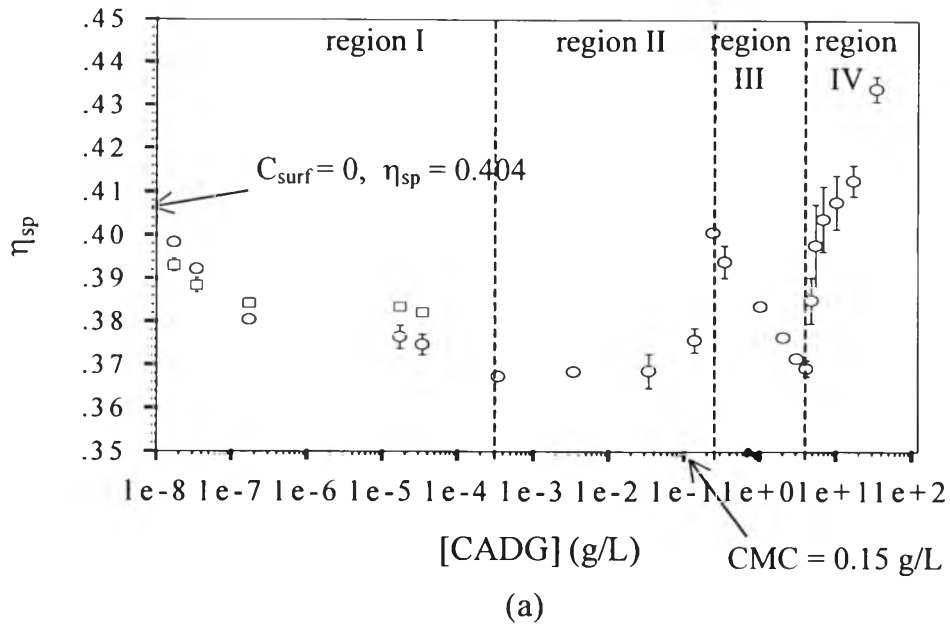
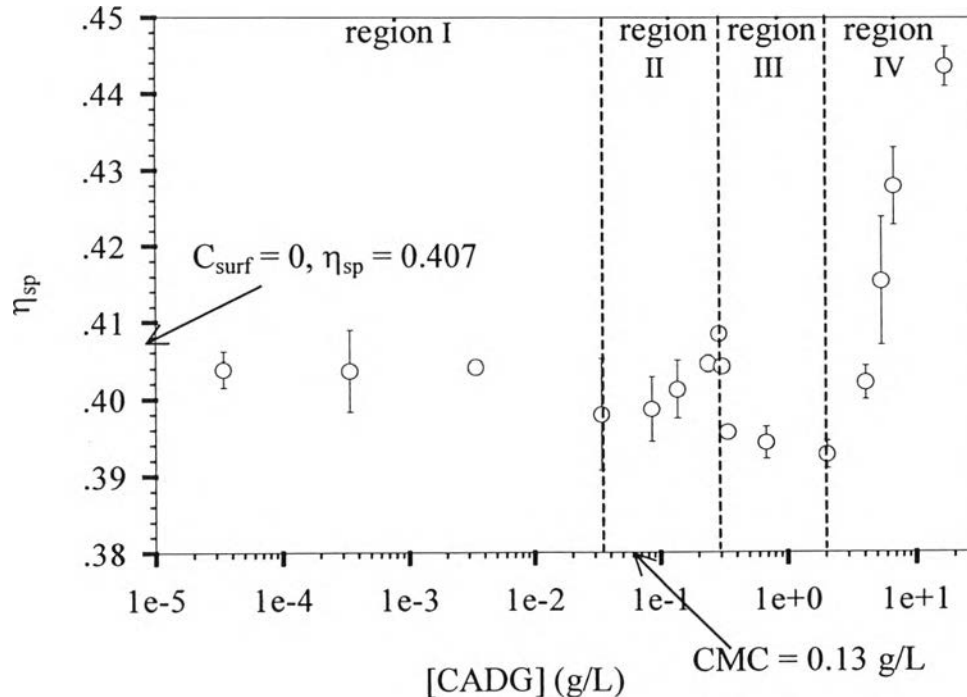
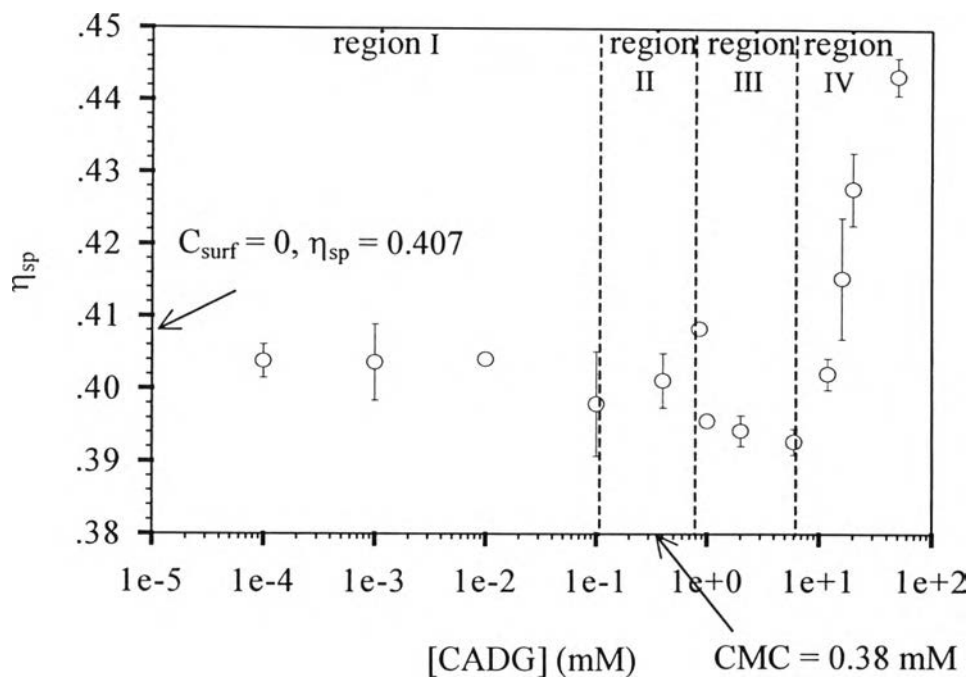


Figure 4.10 The specific viscosity of fixed 2.6 g/L of HPC concentration as a function of CADG concentration at 30°C of HPC/CADG/water system at pH 12.0: (○) Ubbelodhe capillary viscometer size 50, (□) Ubbelodhe capillary viscometer size 25, (a) CADG concentration in g/L; (b) CADG concentration in mM.

Figure 4.11 shows the specific viscosity of the HPC/CADG/water system at pH 9.0 as a function of CADG concentration, the HPC concentration is fixed at 2.6 g/L. This figure can also be divided into four regions. In region I, the CADG concentration is between 3.42×10^{-5} g/L and 0.034 g/L and the specific viscosity slightly decreases from 0.404 to 0.398. In region II, the specific viscosity slightly increases from 0.398 to 0.408 when the CADG concentration increase from 0.034 g/L to 0.29 g/L. In region III, the CADG concentration increases from 0.29 g/L to 2.05 g/L, the specific viscosity decreases from 0.408 to 0.394. Above 2.05 g/L, the specific viscosity rapidly increases as a function of CADG concentration. The maximum specific viscosity of about 0.408 or the maximum binding point occurs at the CADG concentration of about 0.29 g/L.



(a)



(b)

Figure 4.11 The specific viscosity of fixed 2.6 g/L of HPC concentration as a function of CADG concentration at 30°C of HPC/CADG/water system at pH 9.0: (a) CADG concentration in g/L; (b) CADG concentration in mM.

4.2.2 Hydrodynamic Radius Determination

Figure 4.12 shows the apparent diffusion coefficient, D_{app} , for the HPC/CADG/water system at pH 3.0 as a function of scattering wave vector square, q^2 , at scattering angles from 70° to 140°. The HPC concentration was fixed at 2.6 g/L.

The hydrodynamic radius of the HPC/CADG/water system at pH 3.0 was calculated using the Stokes-Einstein equation as shown in Figure 4.13 as a function of CADG concentration. The results are consistent with those of the viscosity measurement. At very low concentration of CADG,

the hydrodynamic radius of HPC chain slightly decreases because of the chain contraction. With further addition of CADG, the hydrodynamic radius increases due to the formation of complex between HPC and CADG. After that, the hydrodynamic radius sharply decreases as a function of CADG concentration due to the screening effect of counterions.

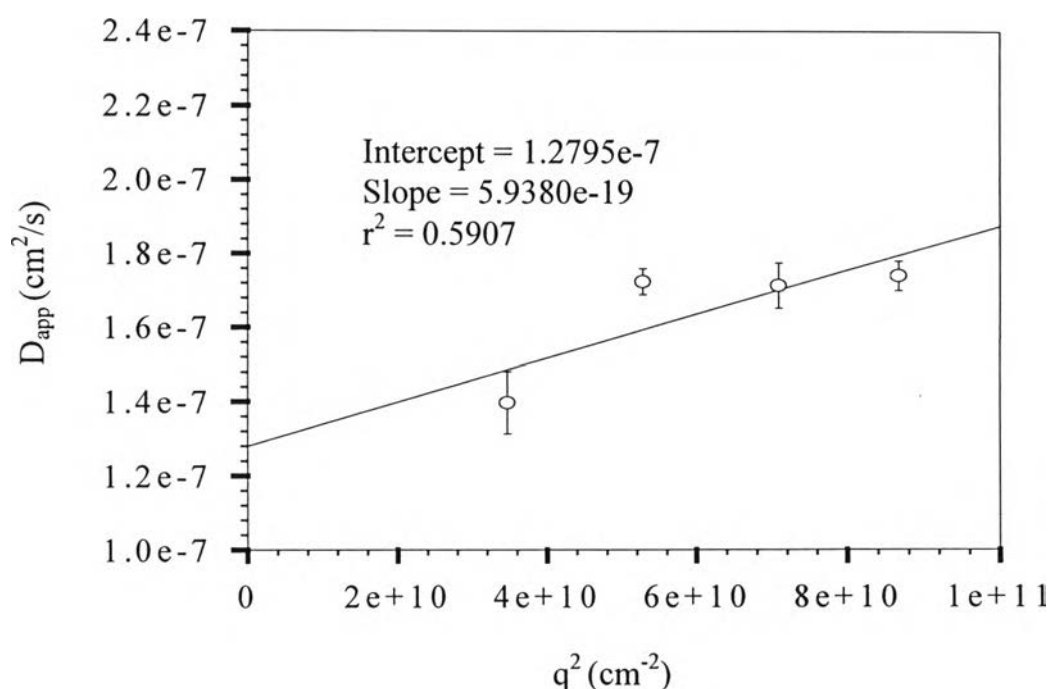
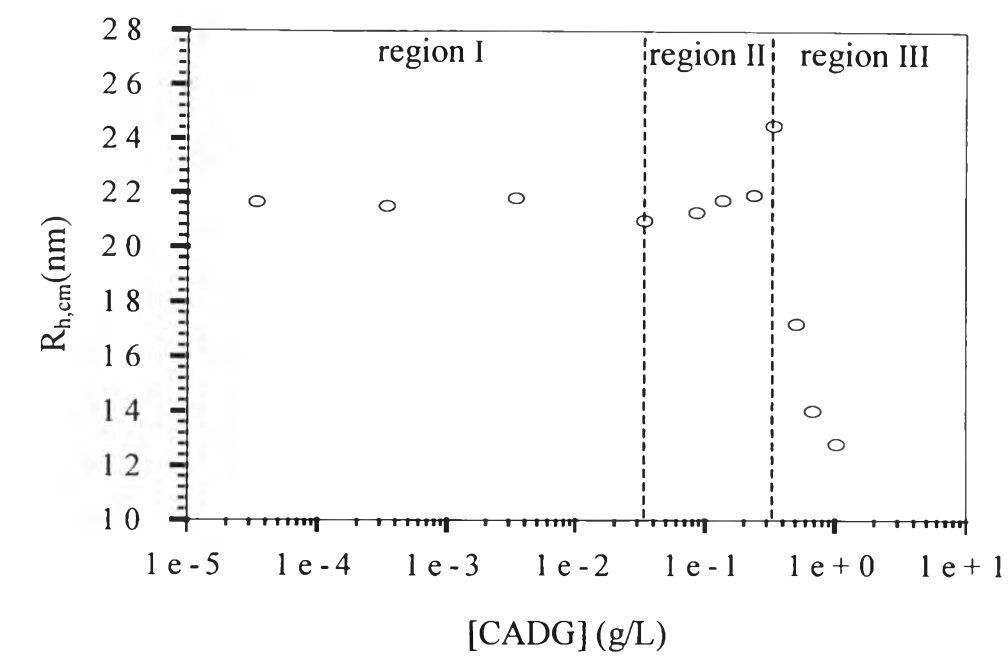
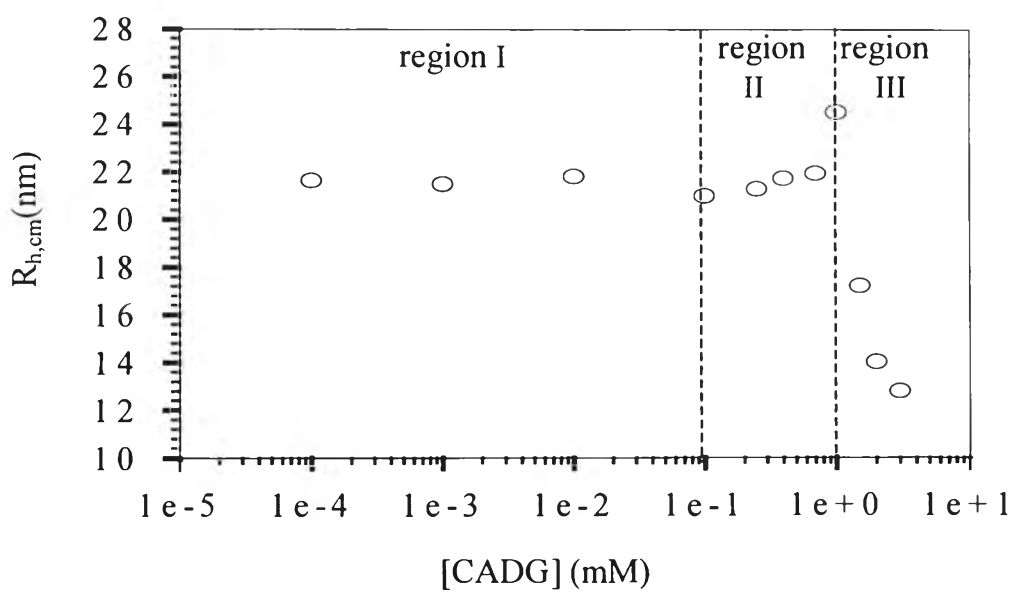


Figure 4.12 Apparent diffusion coefficient for the HPC/CADG/water system at pH 3.0 as a function of the scattering wave vector at 30°C. The HPC concentration and CADG concentration were fixed at 2.6 g/L and 3.42e-5 g/L (1.0e-4 mM).



(a)



(b)

Figure 4.13 R_h of HPC/CADG/water system at pH 3.0 as a function of CADG concentration at 30°C: (a) CADG concentration in g/L; (b) CADG concentration in mM. The HPC concentration was fixed at 2.6 g/L.

4.2.3 Polydispersity Determination

Figure 4.14 shows the polydispersity, $(\Gamma/\langle\Gamma\rangle)^2$, for the HPC/CADG/water system at pH 3.0 as a function of scattering wave vector square, q^2 , at scattering angles from 70° to 140° . The HPC concentration was fixed at 2.6 g/L. Similar plots for other HPC/CADG/water systems are shown in appendix C. Figure 4.15 shows the variation of $(\Gamma/\langle\Gamma\rangle)^2$ for the HPC/CADG/water system at pH 3.0 as a function of CADG concentration.

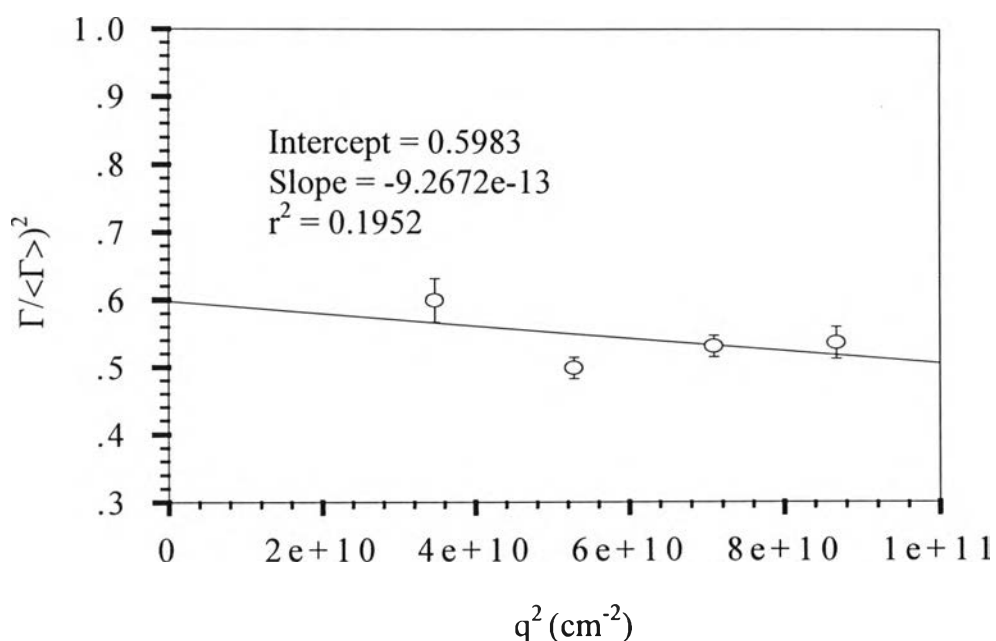
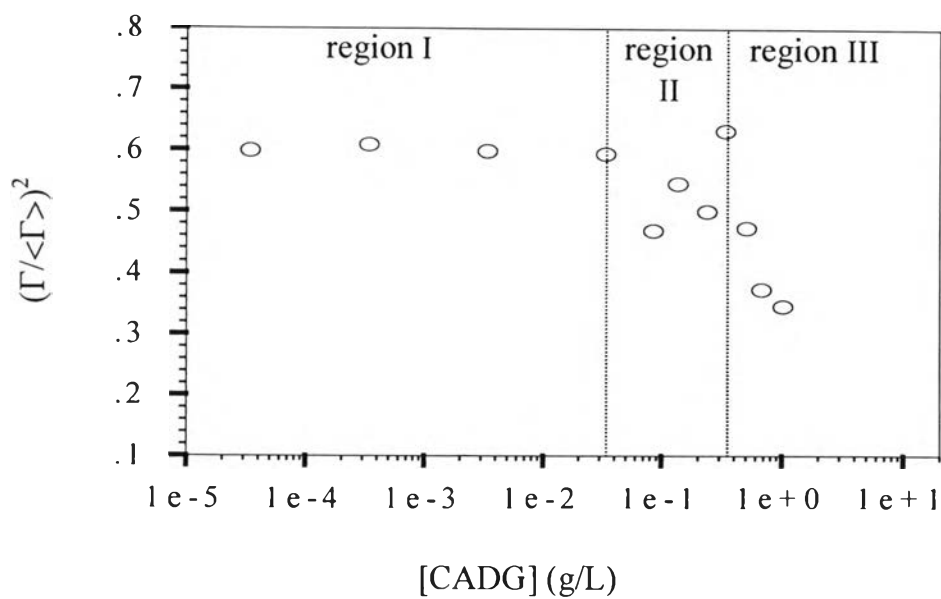
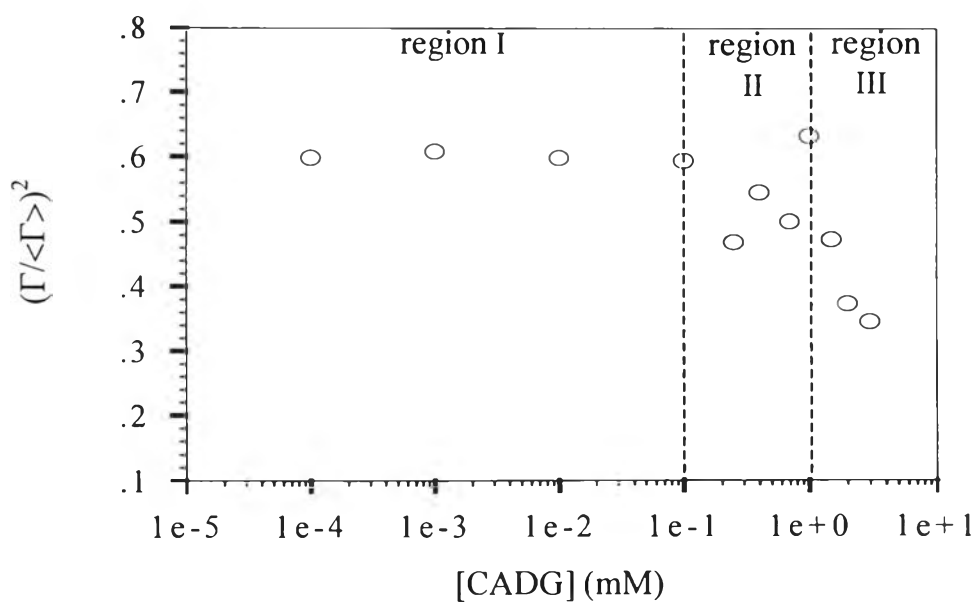


Figure 4.14 Polydispersity for the HPC/CADG/water system at pH 3.0 as a function of the scattering wave vector at 30°C . The HPC concentration and CADG concentration were fixed at 2.6 g/L and $3.42\text{e-}5$ g/L ($1.0\text{e-}4$ mM).



(a)



(b)

Figure 4.15 $(\Gamma/\langle\Gamma\rangle)^2$ of HPC/CADG/water system at pH 3.0 as a function of CADG concentration at 30°C: (a) CADG concentration in g/L; (b) CADG concentration in mM. The HPC concentration was fixed at 2.6 g/L.

Table 4.1 summarises experimental data at the maximum binding point for the HPC/CADG/water system at the three different pH values: pH 3.0, pH 9.0 and pH 12.0. It is interesting to note that, if one assume the initial chain contraction arises because of the decrease in solvent quality due to the present of surfactant, which is different at the three pH values (see Figs. 4.8, 4.10 and 4.11), and therefore estimate the fractional amount of chain expansion at maximum binding as $\eta_{sp,max}/\eta_{sp,min}$, you find ratios of $\eta_{sp,max}/\eta_{sp,min} = 0.428/0.394 = 1.086$, $\eta_{sp,max}/\eta_{sp,min} = 0.408/0.398 = 1.025$, and $\eta_{sp,max}/\eta_{sp,min} = 0.402/0.368 = 1.092$, at pH = 3,9, and 12, respectively. This indicates a minimum in the relative chain expansion at the isoelectric pH, consistent with expectation on the basis that the force between bound micelles near the isoelectric pH will be attractive, in contrast to the repulsive force under strongly cationic or anionic conditions.

Table 4.1 Table of maximum binding point for HPC/CADG/water system at pH 3.0, 9.0, and 12.0.

HPC/CADG/water System	η_{sp}	$R_{h,cm}$ (nm)	[CADG] (g/L)	[CADG] (mM)	$(\Gamma/\langle\Gamma\rangle)^2$
pH 3.0	0.430	24.52	0.34	1.0	0.6321
pH 9.0	0.408	-	0.29	0.85	-
pH 12.0	0.402	-	0.24	0.7	-